J. Fluid Mech. (1966), *vol.* 25, *part* 4, *pp.* 683–704
Printed in Great Britain

On transition in a separated laminar boundary layer

By PETER FREYMUTH

Deutsche Versuchsanstalt für Luft- und Raumfahrt,
Institut für Turbulenzforschung, Berlin 12

(Received 27 September 1965)

This paper deals with the growth of small disturbances in a separated laminar boundary layer for high Reynolds numbers as a function of the dimensionless flow parameters. Using a hot-wire technique, the experiments show that spatially growing disturbances are only affected by the Strouhal number. Thus the basic equations of the process become relatively simple. The experiments show good agreement with theoretical results obtained by means of hydrodynamic stability theory for spatially growing disturbances.

1. Introduction

Laminar steady flow configurations have the tendency to become periodic and finally irregular. This laminar–turbulent transition has been well known since Reynolds's (1883) famous experiments. Many investigations concerning the problem of the growth of small disturbances have since been made. The growth of small disturbances in the flow along a flat plate was investigated successfully by Schubauer & Skramstad (1947), verifying the theory of Tollmien (1929) and Schlichting (1935). However, the transition range from exponentially growing disturbances to fully developed turbulent motion has had no adequate theoretical description. For wall boundary layers there is the theory of vortex instability by Görtler (1940), and for separated laminar layers, such as exist in free jets, Wille (1952, 1960) and Domm (1956) suggested that the transition from exponentially growing waves to fully developed turbulence goes through periodic annular vortices. The vortices break down three-dimensionally and this marks the onset of turbulence. This concept was verified by Wille (1963*a*, *b*), Michalke & Wille (1966), Michalke (1965*a*) and Wehrmann (1957) in laminar separated layers of free jets leaving a nozzle. But in the course of this work the following questions were not answered.

(1) Calculations by Schade & Michalke (1962), Michalke & Schade (1963), and Michalke (1964) concerning the growth of disturbances in separated layers did not agree in all points with the experiments, or the experiments had not been done to verify the calculations. So the influence of the Strouhal number on the growth of the disturbances was not investigated experimentally.

Sato (1956, 1959, 1960), as well as Fabian (1960), found a phase reversal of about 180° in the fundamental component of the velocity fluctuations on traversing the boundary layer with a hot-wire. The stability calculations by Michalke (1964) for temporally growing disturbances did not show such a phase reversal. So the assumptions of these calculations seemed to be uncertain. Timme (1959) and Fabian tried to explain the phase reversal by postulating the existence of vortices.

(2) While vortex models succeeded in the wakes of cylinders, they did not agree with the experiments in separated layers.

(3) The influence of sound on the growth of disturbances was found by Wille (1963*b*) and Michalke & Wille (1966) to be rather complicated and their observations could not be explained. Moreover, the growth of disturbances seemed to depend on the way they were excited. There was no agreement between disturbances excited by sound and disturbances excited by a vibrating ribbon.

(4) Smoke pictures were not correlated with hot-wire signals and the hypothesis of growing vortices could not be verified.

(5) The break down of the vortices could not be explained. Timme (1957) suggested that a critical Reynolds number $\Gamma_{\text{crit.}}/\nu$ of a single vortex was relevant for the break down, and Fabian (1960) applied this hypothesis to the mixing region of a free jet. $\Gamma_{\text{crit.}}$ is a critical circulation of a single vortex and ν is the viscosity. If a vortex had reached this Reynolds number during its growth, it was assumed that the vortex would break down. Obviously viscosity plays an important role in this hypothesis. Domm (1956) proposed that centrifugal instability would be relevant, too, for vortex break down. But there was no proof of the hypotheses by Timme and Domm.

In this paper an attempt is made to clarify, by experimental investigations, the remaining questions relating to the laminar–turbulent transition in a separated layer.

2. Theoretical assumptions and the experimental problem

In this paper the sound-excited laminar–turbulent transition in separated layers formed by a round or plane nozzle is investigated. When excited by sound from a loudspeaker, the boundary layer begins to meander near the nozzle edge and further downstream to roll up into vortices, as can be seen in figure 1 (plate 1). In the further development the vortices 'slip' by mutual induction; i.e. two consecutive vortices circulate around a common axis. The vortices finally approach each other and break up into turbulence.

An attempt is made to describe this process by dimensionless flow parameters. The momentum thickness θ of the layer is chosen as characteristic length and the jet velocity U_0 as characteristic velocity. The basic equations and boundary conditions contain four flow parameters:

(1)	$2P_s/\rho U_0^2$	Pressure number;
(2)	U_0/a	Mach number;
(3)	$U_0\theta/\nu$	Reynolds number;
(4)	$f\theta/U_0$	Strouhal number.

The following symbols are used: p_s, sound pressure; a, velocity of sound; f, sound frequency; ρ, density; ν, viscosity (*circa* 0·15 cm^2 sec^{-1} in air).

In principle the levels of turbulence and noise in the surrounding air must be considered, but the influence of these parameters is suppressed as much as possible by the experimental arrangement. A solution of the system of equations governing the transition process will depend in principle on all four parameters mentioned above. Since it seems to be impossible to obtain a solution theoretically, the depend-

ence of the transition process on the four characteristic hydrodynamic numbers was investigated experimentally. These experiments show that the problem can be simplified.

3. Experimental arrangement and methods

Artificial disturbances in the boundary layer of the jet were excited by sound from a loudspeaker. The growth of the disturbances in the boundary layer was investigated by a hot-wire technique. The experiments showed that the velocity fluctuations contain higher harmonics of the sound frequency which depend in a complicated manner on the position of the hot-wire probe in the layer. Therefore only the fundamental component of the fluctuations was evaluated. This had the additional advantage that small band frequency analysers could be used, and so the evaluation of very small fluctuations was possible without a disturbing influence of the signal-to-noise ratio. In order to interpret the results they were correlated to a 'vortex picture' obtained by introducing smoke into the shear layer and making an instantaneous photograph.

A detailed description of the experimental arrangement is given in the following parts of this section.

3.1. *The test stand*

A radial-flow fan was used to produce a fairly constant pressure in a big settling chamber. On the front plate of this settling chamber the nozzle for the jet was mounted as shown in figure 2 (plate 1). The whole test stand was surrounded by a noise-damping shell to reduce the noise level. The nozzles used in the experiments were axisymmetric 'vortex filament nozzles' described by Michalke (1962), and a plane nozzle. The diameters of the axisymmetric nozzles at the final cross-section were 7·5 cm, 10 cm and 14 cm; the plane jet had an area of 4 cm × 40 cm. The velocity in the jet could be varied from 2 to 32 m/sec. In this velocity range the boundary-layer thickness was very small compared with the nozzle diameter so that the opposite regions of the layer did not interact. For velocity profiles of the separated layer see figures 5 and 29.

3.2. *Hot-wire measurements*

The velocity in the separated layer was measured with a hot-wire anemometer designed by Berger, Freymuth & Froebel (1963*a*, *b*). The hot-wire probe was mounted on a traversing mechanism and could be moved continuously in the jet direction (x-direction) and perpendicular to the jet (y-direction) by means of two synchronous motors. The output voltage of the hot-wire anemometer corresponded linearly to the flow velocity at the position of the hot-wire. This voltage fed a galvanometer recorder (Honeywell, Visicorder) and a frequency analyser (Rohde & Schwarz, FTA) in order to analyse the fundamental component of the periodic fluctuations in the shear layer. The output of the analyser fed another galvanometer of the recorder. In order to measure the phase of the fluctuations relative to the sound generator a phase meter (Rohde & Schwarz, PZN) was used.

The sound for exciting small disturbances in the layer was generated by a loud-speaker mounted above the nozzle or inside the settling chamber some distance

from the nozzle. The loudspeaker was fed by a sine generator. The sound frequency always agreed with the analyser frequency. The sound level was measured by a microphone using a sound level meter. Figure 3 shows a diagram of the measuring equipment.

3.3. *Smoke technique*

Some smoke photographs were made to complete the hot-wire measurements and to correlate them with the flow picture. Stroboscopic light or single flashes of light were used to photograph the smoke pictures. The smoke was introduced into the

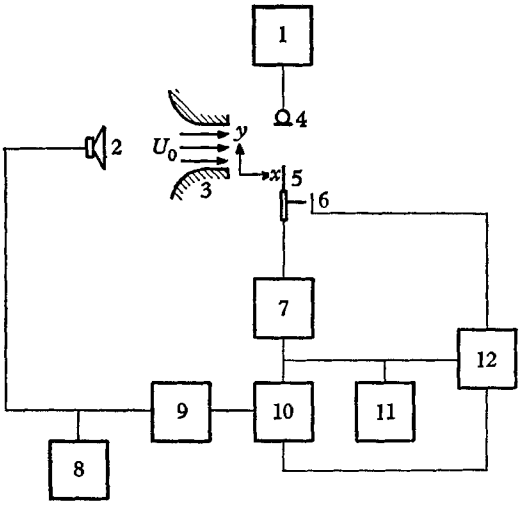

FIGURE 3. Diagram of the measuring arrangement. 1, Sound pressure meter; 2, loudspeaker; 3, nozzle; 4, microphone; 5, hot-wire probe; 6, probe position meter; 7, hot-wire anemometer; 8, frequency meter; 9, sine generator; 10, frequency analyser; 11, oscilloscope; 12, Visicorder galvanometers.

separated layer near the nozzle edge by a smoke pipe (Auer). The growing disturbances could be analysed using hot-wire techniques while a stroboscopic smoke picture could be viewed and photographed simultaneously. A correlation between hot-wire measurements and the smoke picture was thereby obtained. The following considerations made an interpretation of the smoke pictures possible. In a two-dimensional inviscid flow the vorticity transport is described by the Helmholtz equation

$$d\Omega/dt = 0.$$

This means that the vorticity Ω is fixed to the fluid. When smoke is introduced into the layer near the nozzle, the smoke is distributed downstream in the same way as the vorticity in the smoky part of the layer and so the smoke pictures give a fairly good picture of the vorticity distribution in the layer. As the following sections show, the assumptions of two-dimensional and inviscid flow are approximately satisfied.

3.4. *Measuring methods*

3.4.1. *The momentum thickness*

The momentum thickness θ of the separated boundary layer is defined by

$$\theta = \int_{-\infty}^{+\infty} \frac{u}{U_0}\left(1-\frac{u}{U_0}\right) dy,$$

where u is the velocity at the point y in the velocity profile. In practice the integration has to be extended over the thickness of the boundary layer only. θ is a function of the distance x from the nozzle and of the Reynolds number. As can be seen from Schade & Michalke (1962) the boundary-layer theory gives the following formulae

$$\theta R_D^{\frac{1}{2}}/D = f_1(x/D) \quad \text{for axisymmetric nozzles,}$$

$$\theta R_h^{\frac{1}{2}}/h = g_1(x/h) \quad \text{for the plane nozzle,}$$

where $$R_D = U_0 D/\nu \quad \text{and} \quad R_h = U_0 h/\nu,$$

with D the nozzle diameter of the axisymmetric nozzles and h the width of the plane nozzle.

The equations above yield

$$\theta/\theta_0 = f(x/D) \quad \text{for axisymmetric nozzles,}$$

$$\theta/\theta_0 = g(x/h) \quad \text{for the plane nozzle.}$$

θ_0 is the momentum thickness at the nozzle edge, where x is zero. The above results were obtained theoretically; f and g are unknown and so the dependence of the functions f and g on x was determined experimentally, as well as f_1 and g_1 at $x = 0$. The velocity profiles were recorded by a hot-wire equipment for various values of x. It should be noted that the measurements described above were made in the undisturbed shear layer. In the disturbed layer the momentum thickness changes much more rapidly with x owing to the Reynolds stresses, but this was not investigated.

3.4.2. *Analysis of growing disturbances*

For constant jet velocity, sound frequency, and intensity the hot-wire probe was moved through the layer (y-direction) while the x-position remained fixed. The hot-wire signal and the analyser output were recorded. The analyser record will be called the amplitude distribution. The y-scale is fixed on the record by light marks (every $\Delta y = 0{\cdot}2$ mm). As an example, figure 6 (plate 2) shows a record obtained in this way. In the amplitude distribution we see two maxima and a sharp minimum between them; moreover a third maximum may appear further downstream, as shown in figure 7 (plate 2).

The dependence of the amplitude distribution on the distance x from the nozzle was determined by a repetition of the procedure described above for various values of x. The main interest of the investigations by means of hot-wire measurements was the amplitude distribution, but for completeness the phase distribution was measured too.

By variation of the characteristic hydrodynamic parameters their influence on the transition was determined and important insight for a theoretical analysis was found.

4. Experimental results

4.1. *The momentum thickness*

Figure 4 shows the dependence of θ/θ_0 on x for the undisturbed shear layer. θ/θ_0 depends slightly on x close to the nozzle, and is fairly independent of x further downstream. In this region the conversion of the asymmetric wall boundary-layer

profile into the nearly antisymmetric free shear layer takes place. Since the transition was only investigated in the antisymmetric region of the shear layer, the value of θ at the position $x_m/D = 0{\cdot}026$ and $x_m/h = 0{\cdot}045$ respectively was chosen as the characteristic length θ_m of the problem. The following relations for θ_m were found:

$$\theta_m R_D^{\frac{1}{2}}/D = 0{\cdot}61, \quad \theta_m R_h^{\frac{1}{2}}/h = 0{\cdot}82.$$

4.2. *Experimental results concerning the growth of disturbances*

Before describing the experimental results in detail, a general description of the amplitude distribution as a function of x is given, because it is qualitatively the same for all combinations of the hydrodynamic parameters.

If the separated layer near the nozzle edge is traversed with a hot-wire, an amplitude distribution (caused by the sound of the loudspeaker) with only one maximum is found, as is shown in figure 5 (plate 2).

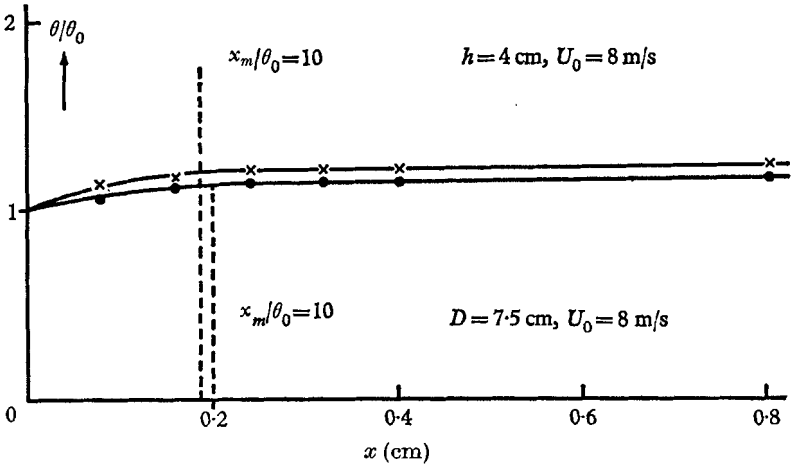

FIGURE 4. Dependence of the momentum thickness θ on the distance x from the nozzle. ×, Plane nozzle; ●, axisymmetric nozzle.

Figure 6 (plate 2) shows the velocity fluctuations and the amplitude distribution further downstream. Here the velocity fluctuations have changed so that the amplitude distribution shows two maxima with a sharp minimum between them. The two maxima are growing with increasing distance x from the nozzle. But later on a third maximum appears, growing from the right flank of the second maximum (figure 7, plate 2), and still further downstream the second maximum coalesces with the third (figure 8, plate 3). Finally at the onset of turbulence the velocity fluctuations become irregular, so that it is impossible to analyse the records (figure 9, plate 3), which no longer show reproducible amplitude distributions. In the following parts of this section the three characteristic maxima of the amplitude distribution $\hat{c}_{1,2,3}/U_0$ and their distances $d_{1,2,3}/\theta_m$ from the sharp minimum were analysed as a function of x/θ_m. The velocity maxima were plotted on a logarithmic scale. In order to study the dependence of the disturbance amplification on the hydrodynamic parameters, only one of them was varied at a time, while the others were kept constant or were varied only if it had already been found that the flow was independent of them.

4.2.1. *Dependence of $\hat{c}_2/U_0$ on pressure number*

The influence of sound pressure on the amplification is considered first. In figure 10 the dependence of the main maximum $\hat{c}_2/U_0$ on x/θ_m is represented on a logarithmic scale for various sound pressures. The velocity U_0 and the sound

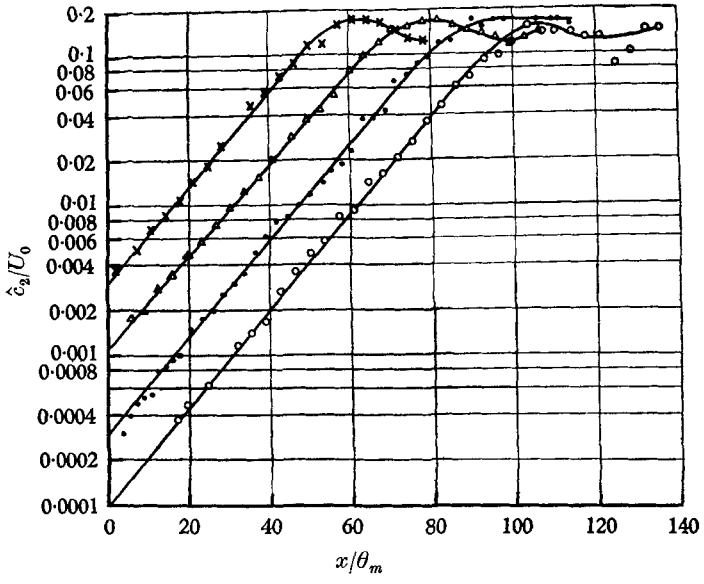

FIGURE 10. Dependence of the growth $\hat{c}_2/U_0$ on the sound pressure. $D = 7{\cdot}5$ cm, $U_0 = 8$ m/sec, $R_\theta = 122$, $S = 0{\cdot}0118$. ○, 70 dB; ●, 80 dB; △, 90 dB; ×, 100 dB.

frequency f were kept constant. The nozzle diameter was $D = 7{\cdot}5$ cm. The curves in figure 10 are linear in a large region and equidistant. Thus the velocity fluctuations grow exponentially with x in this region, and they are proportional to the sound pressure. We therefore can write for this linear range:

$$\hat{c}_2/U_0 \sim (2p_s/\rho U_0^2)\exp(a'x/\theta_m).$$

The fluctuations subsequently reach a maximum and then decrease slowly till the curves are no longer defined, because the maximum $\hat{c}_2$ coalesces with the maximum $\hat{c}_3$.

4.2.2. *Dependence of $\hat{c}_2/U_0$ on the Mach number*

The maximum $\hat{c}_2/U_0$ as a function of x/θ_m for various pressure numbers is shown again in figure 11. But now the pressure number was varied by variation of U_0 while keeping p_s proportional to U_0. This yields:

$$\frac{p_s}{\frac{1}{2}\rho U_0^2} \sim \frac{1}{U_0}.$$

On the other side the sound frequency f was chosen so that the Strouhal number $S = 0{\cdot}0118$ was constant. From the linear region of the curves it follows that

$$\frac{\hat{c}_2}{U_0} \sim \frac{p_s}{\frac{1}{2}\rho U_0^2}\exp(a'x/\theta_m).$$

Although the Mach number was varied by changing U_0, we obtain the same results as in the previous section. Thus it follows that the Mach number has no effect on the transition for this velocity range. Figures 10 and 11 show that the pressure number

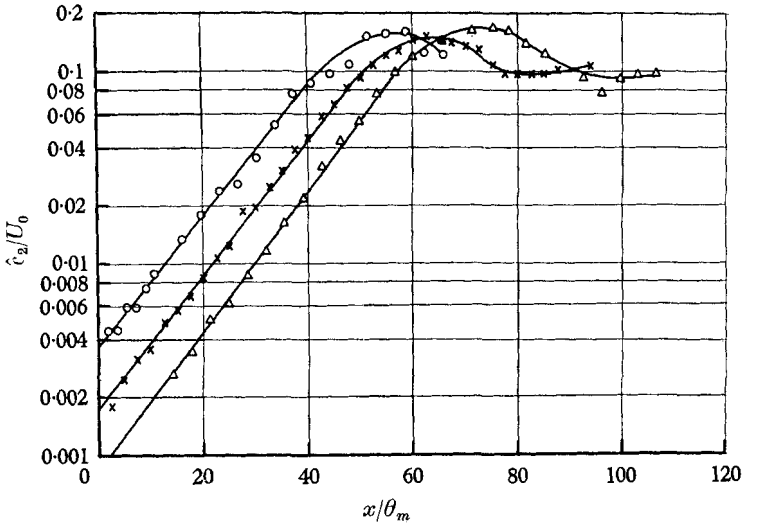

FIGURE 11. Dependence of the growth of $\hat{c}_2/U_0$ on the sound pressure and the jet velocity. $D = 7{\cdot}5$ cm, $S = 0{\cdot}0118$. ○, 8 m/sec, 90 dB; ×, 16 m/sec, 96 dB; △, 32 m/sec, 102 dB.

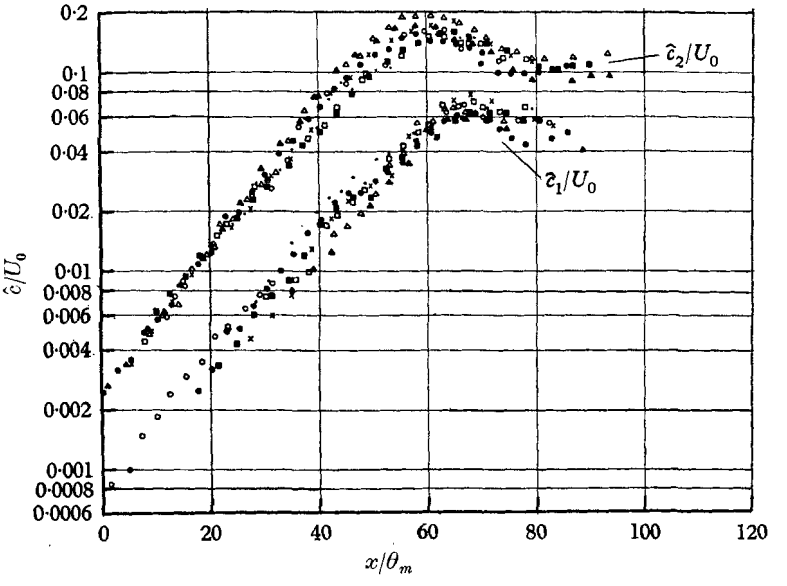

FIGURE 12. Dependence of the growth of $\hat{c}_1/U_0$ and $\hat{c}_2/U_0$ on the Reynolds number. $S = 0{\cdot}0118$. ●, $R_\theta = 61$; □, $R_\theta = 86$; ○, $R_\theta = 122$; ■, $R_\theta = 141$; ●, $R_\theta = 173$; ×, $R_\theta = 236$; ▲, $R_\theta = 244$; △, $R_\theta = 334$.

only causes a shift of the amplification curves without deformation. Thus we conclude that the amplification is independent of $p_s/\frac{1}{2}\rho U_0^2$. This number only determines the amplitude of the disturbances at the nozzle edge, from which the transition starts. Introducing a normalized origin at the x-axis all curves can be

made to coincide. The point where the maximum $\hat{c}_2/U_0$ reaches the value 0·0025 was chosen as normalized origin of the x-axis. The normalized curves are independent of the position of the loudspeaker.

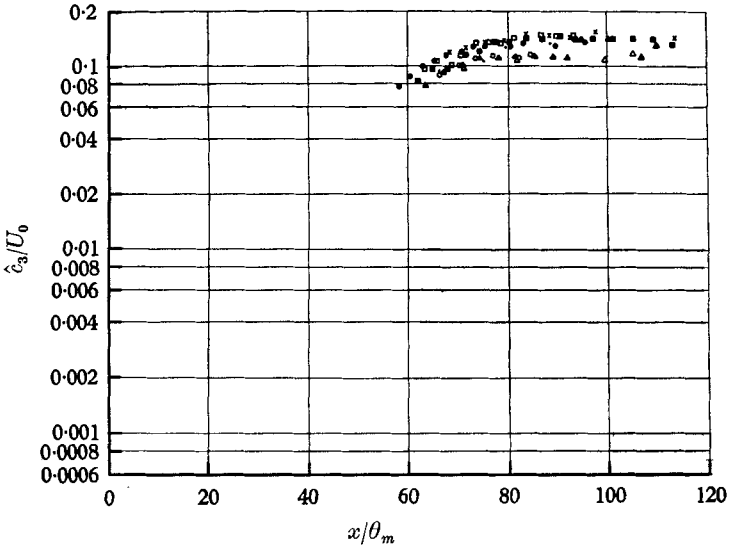

FIGURE 13. Dependence of the growth of $\hat{c}_3/U_0$ on the Reynolds number. S = 0·0118. ●, R_θ = 61; □, R_θ = 86; ○, R_θ = 122; ■, R_θ = 141; ●, R_θ = 173; ×, R_θ = 236; ▲, R_θ = 244; △, R_θ = 334.

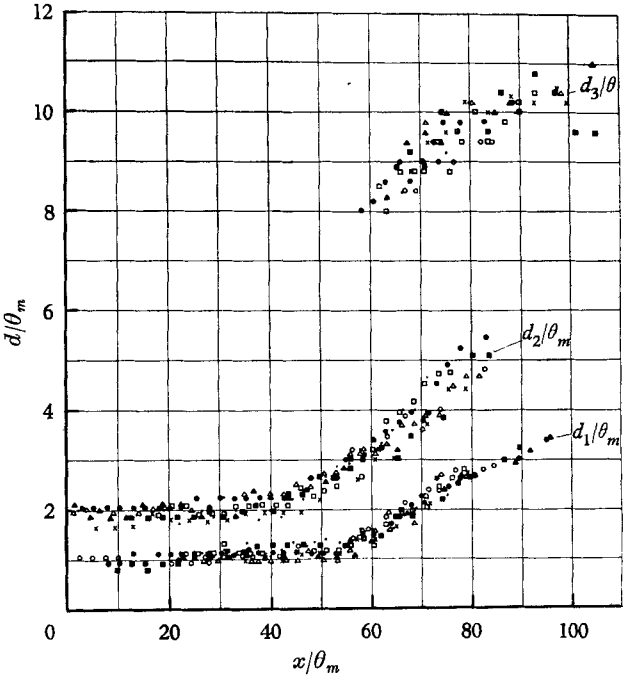

FIGURE 14. Dependence of the distances $d_{1,2,3}/\theta_m$ on the Reynolds number. S = 0·0118. ●, R_θ = 61; □, R_θ = 86; ○, R_θ = 122; ■, R_θ = 141; ●, R_θ = 173; ×, R_θ = 236; ▲, R_θ = 244; △, R_θ = 334.

4.2.3. *Dependence of the transition on the Reynolds number*

Figure 12 shows the dependence of $\hat{c}_1/U_0$ and $\hat{c}_2/U_0$ on the Reynolds number $R_\theta = U_0\theta_m/\nu$ in the normalized system; figure 13 shows the same for $\hat{c}_3/U_0$. Figure 14 shows the corresponding distances $d_{1,2,3}/\theta_m$ from the sharp minimum. The Reynolds

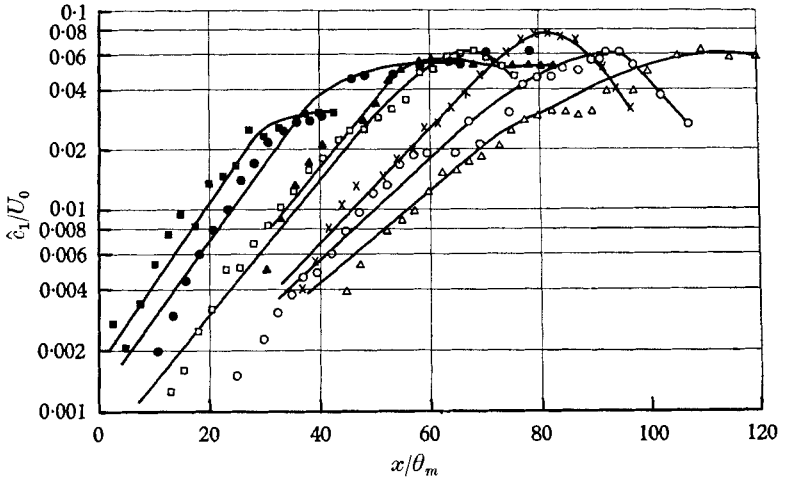

FIGURE 15. Dependence of the growth of $\hat{c}_1/U_0$ on the Strouhal number. D = 7·5 cm, U_0 = 16 m/sec. △, S = 0·0080; ○, S = 0·0090; ×, S = 0·0100; □, S = 0·0118; ▲, S = 0·0148; ●, S = 0·0177; ■, S = 0·0236.

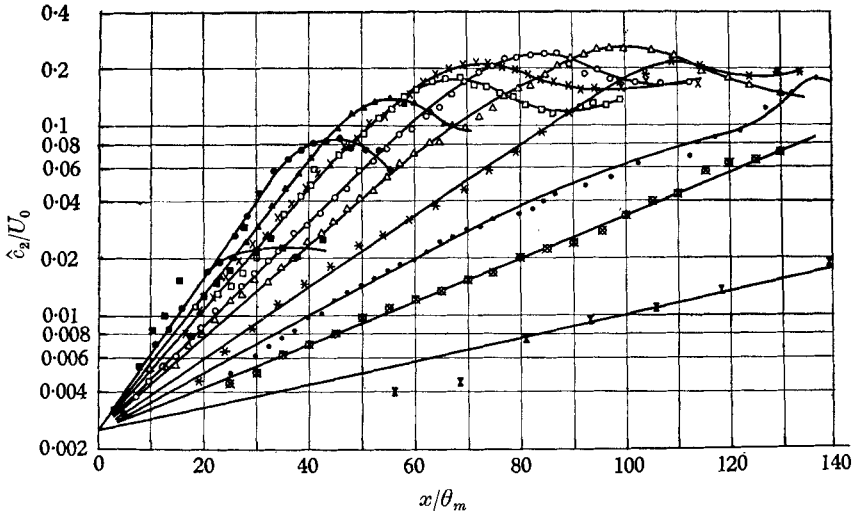

FIGURE 16. Dependence of the growth of $\hat{c}_2/U_0$ on the Strouhal number. D = 7·5 cm, U_0 = 16 m/sec. □, S = 0·0118; ▲, S = 0·0148; ●, S = 0·0176; ■, S = 0·0234; ⧗, S = 0·0020; ⊠, S = 0·0040; •, S = 0·0050; *, S = 0·0070; △, S = 0·0080; ○, S = 0·0090; ×, S = 0·0100.

number was varied over the range $61 \leqslant R_\theta \leqslant 334$ by variation of the velocity ($U_0 = 2 \ldots 32$ m/sec) and of the nozzle diameter (D = 7·5; 10; 14 cm). We see that within an accuracy of ± 10 % the transition is independent of the Reynolds number, and therefore we can treat the flow as inviscid.

4.2.4. *Dependence of the transition on the Strouhal number*

§ 4.2.1 to 4.2.3 show that the pressure number, the Mach number and the Reynolds number have no important effect on the transition. Let us now consider the influence of the Strouhal number. The Strouhal number $S = f\theta_m/U_0$ was varied by changing the sound frequency f while U_0, D and p_s were kept constant.

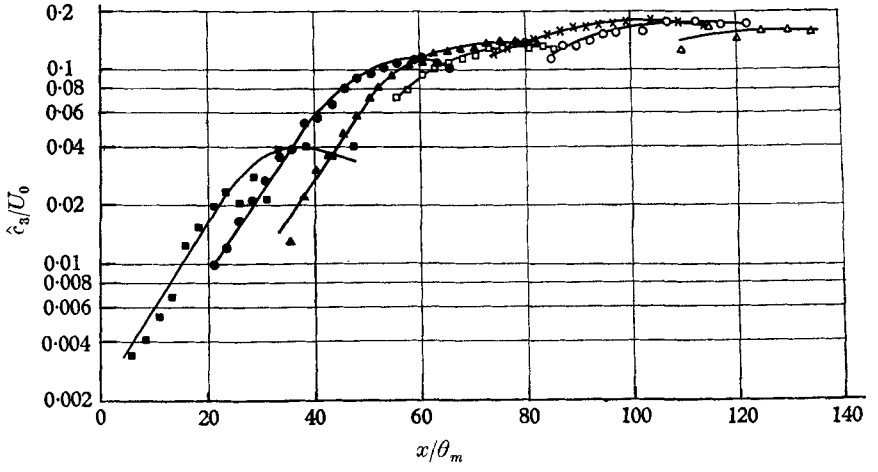

FIGURE 17. Dependence of the growth of $\hat{c}_3/U_0$ on the Strouhal number. D = 7·5 cm, U_0 = 16 m/sec. △, S = 0·0080; ×, S = 0·0090; ○, S = 0·0100; □, S = 0·0118; ▲, S = 0·0148; ●, S = 0·0177; ■, S = 0·0236.

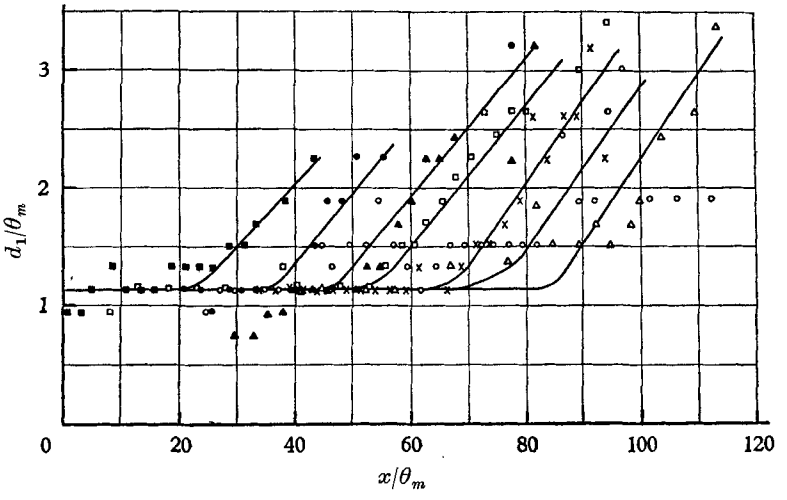

FIGURE 18. Dependence of the distance d_1/θ_m on the Strouhal number. D = 7·5 cm, U_0 = 16 m/sec. △, S = 0·0080; ○, S = 0·0090; ×, S = 0·0100; □, S = 0·0118; ▲, S = 0·0148; ●, S = 0·0178; ■, S = 0·0236.

Figures 15 to 17 show the dependence of the amplification curves $\hat{c}_{1,2,3}/U_0$ on the Strouhal number, figures 18 to 20 the corresponding distances $d_{1,2,3}/\theta_m$. In addition, the transition curves $\hat{c}_2/U_0$ for the plane nozzle are shown in figure 21. Figures 15 to 17 show that with increasing Strouhal number the maxima $\hat{c}_1$ and $\hat{c}_3$ become

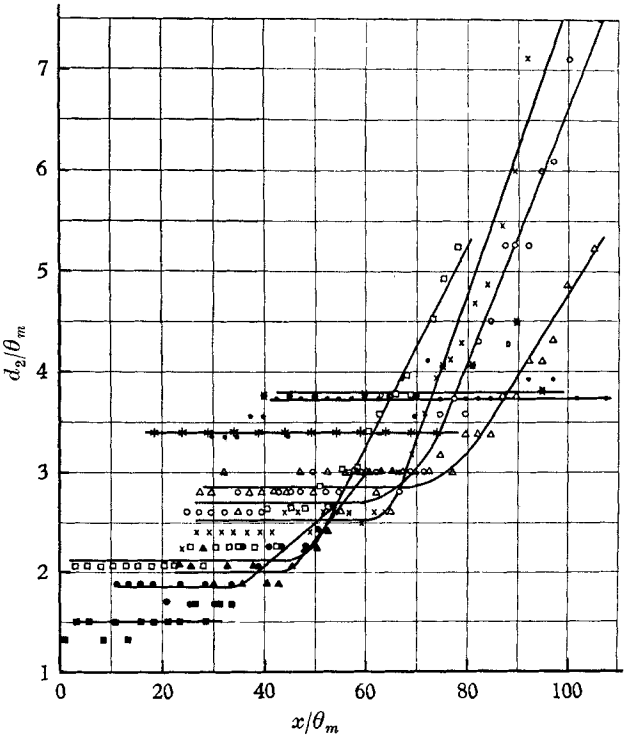

FIGURE 19. Dependence of the distance d_2/θ_m on the Strouhal number. $D = 7{\cdot}5$ cm, $U_0 = 16$ m/sec. ⊗, $S = 0{\cdot}0040$; ●, $S = 0{\cdot}0050$; *, $S = 0{\cdot}0070$; △, $S = 0{\cdot}0080$; ○, $S = 0{\cdot}0090$; ×, $S = 0{\cdot}0100$; □, $S = 0{\cdot}0118$; ▲, $S = 0{\cdot}0148$; ●, $S = 0{\cdot}0177$; ■, $S = 0{\cdot}0236$.

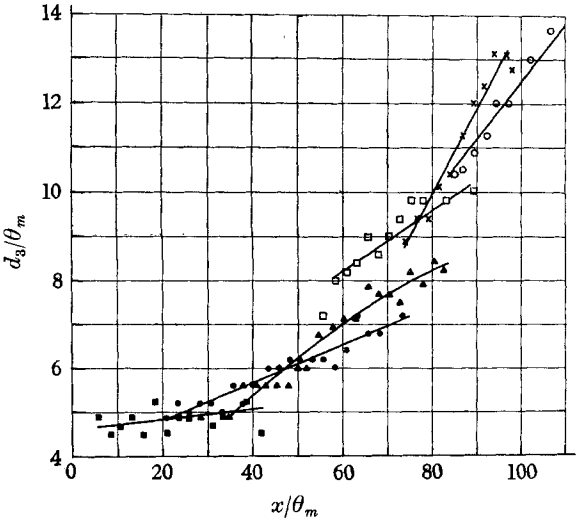

FIGURE 20. Dependence of the distance d_3/θ_m on the Strouhal number. $D = 7{\cdot}5$ cm, $U_0 = 16$ m/sec. ○, $S = 0{\cdot}0090$; ×, $S = 0{\cdot}0100$; □, $S = 0{\cdot}0118$; ▲, $S = 0{\cdot}0148$; ●, $S = 0{\cdot}0178$; ■, $S = 0{\cdot}0236$.

larger relative to $\hat{c}_2$, as can be seen more clearly in figure 22 which shows the ratio of $\hat{c}_1/\hat{c}_2$ in the linear region as a function of S.

The distances $d_{1,2}/\theta_m$ of the maxima from the sharp minimum are independent of x in the linear region and grow linearly with x in the non-linear region, as we see

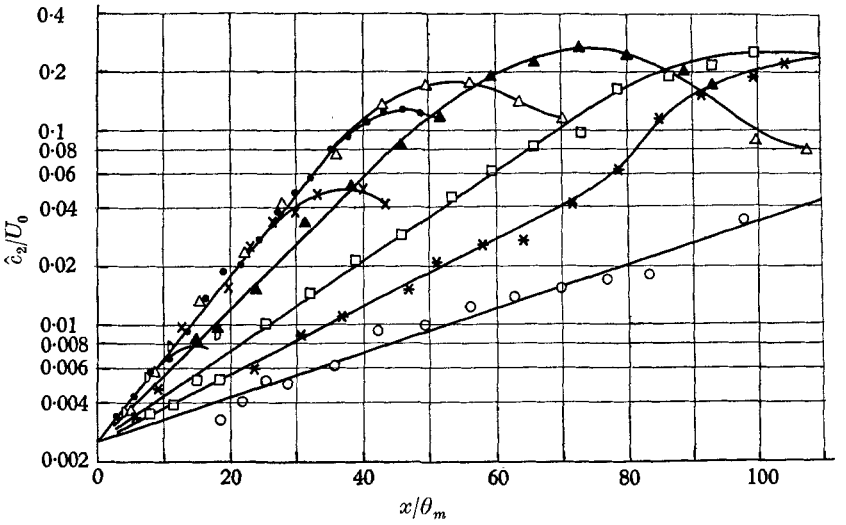

FIGURE 21. Dependence of the growth of $\hat{c}_2/U_0$ on the Strouhal number for the plane nozzle. $h = 4$ cm, $U_0 = 8$ m/sec. ○, $S = 0{\cdot}0034$; *, $S = 0{\cdot}0050$; □, $S = 0{\cdot}0070$; ▲, $S = 0{\cdot}0084$; △, $S = 0{\cdot}0109$; ●, $S = 0{\cdot}0146$; ×, $S = 0{\cdot}0178$; ▯, $S = 0{\cdot}0218$.

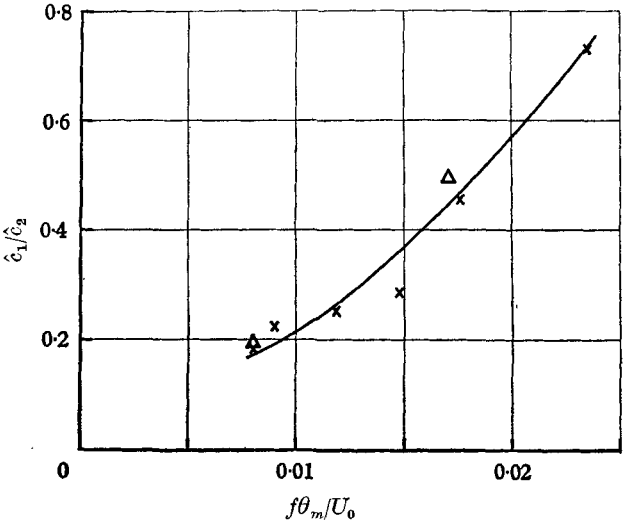

FIGURE 22. Ratio of $\hat{c}_1/\hat{c}_2$ depending on the Strouhal number. △, Calculated values; ×, measured values.

in figures 14, 18 and 19. Axisymmetric and plane nozzles lead to the same results, and therefore only one characteristic length, e.g. the momentum thickness θ_m, is needed. The nozzle diameter D and the slit height h of the plane nozzle are unimportant for the transition in the investigated range of the Reynolds number.

Wavelength measurements for axisymmetric and plane nozzles show the same results (cf. figure 23). The theoretical curves presented in figure 23 together with the experimental results are discussed in § 6.

4.2.5. *Phase measurements*

In addition to the analysis of the amplitude distribution the phase shift and the wavelength were measured. Qualitatively there are no differences between the phase-shift curves for various Strouhal numbers. Quantitative evaluations of the phase distribution were not made in this investigation, and so one phase distribution curve may suffice (figure 24, plate 4).

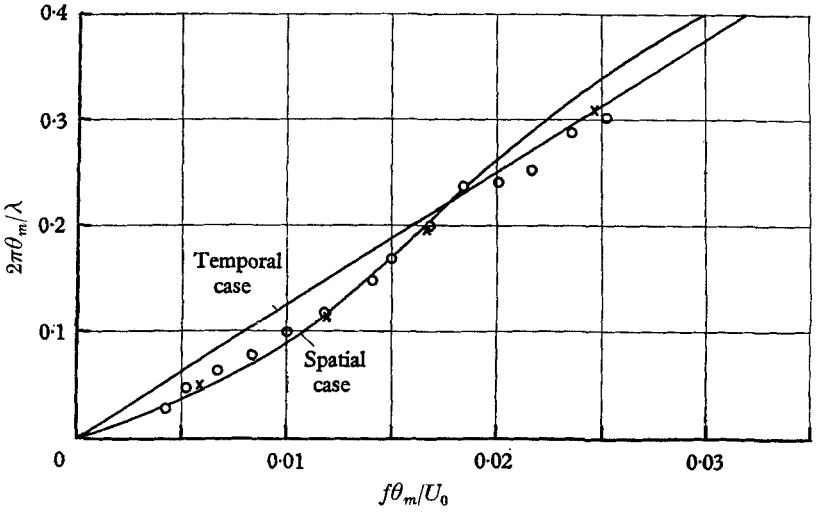

FIGURE 23. Non-dimensional wave-number *vs.* Strouhal number. $U_0 = 8$ m/sec. ○, Axisymmetric nozzle; ×, plane nozzle.

On traversing the hot-wire from the outer part of the jet boundary layer, the following facts were found: At first there is only a little change in the phase, but, when the minimum of the amplitude distribution is reached, a steep phase reversal of about 180° occurs. In the inner part of the layer a continuous phase shift was found.

4.3. *Correlation of smoke pictures to the hot-wire analysis*

As can be seen in § 3.3, smoke pictures give a good impression of the structure of the vorticity distribution.

Figure 25 (plate 5) shows the rolling-up process of vortices excited by sound ($S = 0{\cdot}0118$; $U_0 = 3$ m/sec; $D = 7{\cdot}5$ cm). The interval between the pictures is $\frac{1}{6}$ of the period of the sound. The smoke was introduced into the outer part of the layer. We see in figure 25 that there is a region near the nozzle where the layer is slightly sinuous. Further downstream we find a region where the vortices roll up, and eventually they break down. Comparing the smoke picture and the hot-wire analysis for the same instant, we find the relationship shown in figure 26 (plate 4). The most important result of this correlation is that the two maxima of the amplitude distribu-

tion and also the phase reversal at the sharp minimum occur in the sinuous region. Furthermore, this is the region where the disturbances grow exponentially. But from the smoke picture we see that vortices certainly do not exist there. Therefore we cannot infer the existence of vortices, as did Timme and Fabian, from the existence of a phase reversal of the velocity fluctuations.

In order to see the vorticity distribution in all parts of the layer the smoke was introduced at various heights, as shown in figure 27 (plate 6).

Figure 28 (plate 7) shows that the geometric dimensions of the vortices depend on the Strouhal number, which agrees with the hot-wire analysis shown in figures 19 to 20.

Figure 1 (plate 1) gives an impression of 'vortex slipping' which apparently always exists in the vortex region. A Fourier component at half the sound frequency then appears in the velocity fluctuations.

5. Interpretation of the experimental results

5.1. *The four regions of transition*

The experimental results of § 4 suggest a classification of the transition into four regions, which is useful for an understanding of the mechanism of transition. This classification partially agrees with that proposed by Sato (1959) and is represented in figure 26 (plate 4). Transition excited by sound begins very near the nozzle edge. In this region only one maximum exists in the amplitude distribution, and apparently a transformation of the disturbances takes place so that in the following region an exponential growth is possible. The transformation of the wall boundary layer into the free jet boundary layer also takes place in this region. This region therefore may be called the transformation region.

Further downstream the disturbances grow exponentially, and we find two maxima in the amplitude distribution. This region of 'linear transition' (linear on a logarithmic scale) is followed by a third region which may be called the non-linear region, characterized by vortices in the smoke picture. The amplitude has at first three maxima, and later on two of them coalesce to a single one. In the non-linear region the distance between the maxima is growing. Both the regions of linear and non-linear transition represent the region of laminar–turbulent transition and are followed by a fourth, turbulent region.

The transformation region where compressibility (the initial disturbances are excited by sound) and viscosity are not negligible was not investigated, because the structure of the disturbances in this region has no effect on that of the following regions. This made the investigations in the following regions possible.

5.2. *Reduction of the basic equations*

From the experimental results in § 4 some theoretical assumptions were obtained. As was shown in §§ 4.2 and 4.3, the influence of sound on the transition is restricted to the transformation region and can be eliminated in the following regions by choosing the origin of the x-axis appropriately. The sound determines only the fluctuation amplitude near the nozzle edge, and the amplitude of the disturbances grows exponentially with x in the following linear region. Brown (1935) supposed

the influence of sound to be restricted to the nozzle edge for thin free jets. From the exponential growth of the disturbances it follows that this region can be described by a linear stability theory (see, for instance, Schade 1962).

§ 4.2.3 has shown that the Reynolds number has no important influence in the linear and the non-linear transition region and on the onset of turbulence. The viscosity is only important in the transformation region where the wall boundary-layer profile is transformed into the nearly antisymmetric velocity profile of the free separated layer.

The reduction of the characteristic flow parameters to the Strouhal number alone allows the application of incompressible inviscid stability theory for two-dimensional flow. A linearized theory with exponential growth of the disturbances with x and with a dimensionless frequency S will describe the problem in the linear region. The velocity profile of the basic flow is antisymmetric.

5.3. *Conclusions from the reduced problem*

The experiments and the reduced equations show the spatial character of the problem. The fluctuations grow with x. Thus a theory of spatially growing disturbances should be used, as was proposed by Watson (1962). In the past, theoretical results by Michalke & Wille (1966) and Michalke (1964, 1965*a*) using temporally growing disturbances were used for comparison with experimental results. It was assumed that the results of the temporal problem can be transformed by means of the disturbance phase velocity into that of the spatial problem, an assumption already made by Schubauer & Skramstad (1947) and Sato (1959, 1960). But the experiments described in § 4.2 clearly show that the temporal theory cannot even describe the experiments in the linear range. In particular the asymmetric amplitude distribution, the phase reversal, and their complicated dependence on the Strouhal number are not compatible with the temporal theory, which yields a symmetric amplitude distribution and a monotonic phase distribution. It was supposed in the past that the difference between theory and experiments was caused by the influence of viscosity on the development with x of the boundary-layer velocity profile. But § 4.1 showed the change of the velocity profile is only important in the transformation region, and not in the region of laminar–turbulent transition. So it was suggested that the discrepancy between the results of the temporal theory and of the experiments might be caused by the fact that the transformation of theoretical results obtained for the temporal case into that for the spatial case is not correct; this was already shown by Gaster (1962, 1965). The investigations reported here were originally only undertaken to stimulate the spatial analysis of the problem. But in the meantime a stability calculation for spatially growing disturbances was made by Michalke (1965*b*). By means of his results the amplitude distribution and the phase distribution for spatially growing disturbances was computed by the author, using a digital computer. These calculations and their comparison with the experiments are described in § 6.

6. Theory of spatially growing disturbances and its comparison with the experiments

6.1. *Theory of spatially growing disturbances*

The experiments mentioned above had shown that only a spatial theory could describe the instability of a separated layer. Michalke (1965*b*) succeeded in calculating the stability characteristics of spatially growing disturbances. His calculations and those of the author to determine the amplitude and phase distribution will now be described briefly.

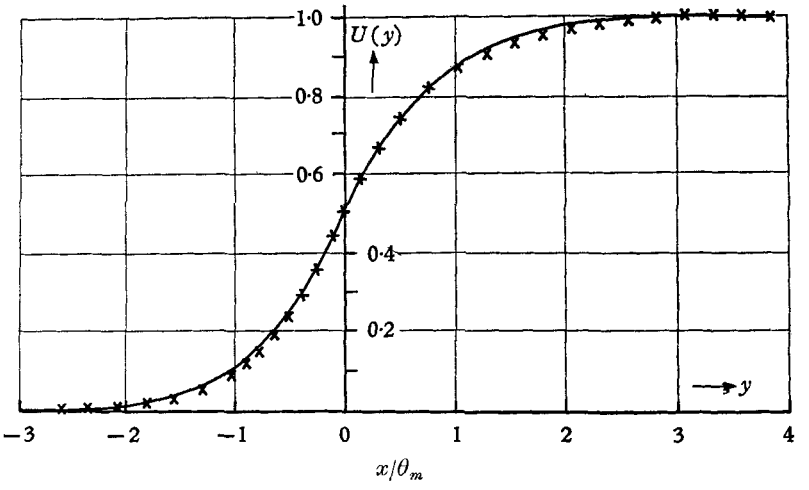

FIGURE 29. Tanh-profile and measured velocity profile in dimensionless form. $D = 7{\cdot}5$ cm, $U_0 = 8$ m/sec, $x/\theta_m = 10$.

Let us assume a two-dimensional unidirectional inviscid flow given by the basic velocity $U(y)$ and a small periodic disturbance given by the stream function†

$$\psi(x,y,t) = \epsilon\mathscr{R}[\phi(y)\,e^{i(\alpha x-\beta t)}].$$

Here ϵ is a measure of the disturbance magnitude, and α and β are constants. Then from the Euler equation of motion we obtain the linearized disturbance equation of Rayleigh:

$$[U-\beta/\alpha][\phi''-\alpha^2\phi]-U''\phi = 0,$$

where the primes denote differentiation with respect to y. For the temporally growing disturbances β is complex and α real, whereas for spatially growing disturbances $\beta = 2\pi S$ must be real and α complex:

$$\alpha = \alpha_r + i\alpha_i;$$

the antisymmetric hyperbolic-tangent profile was chosen as the undisturbed velocity profile $U(y)$ for the calculations. This profile is in good agreement with the experimental velocity profile, as figure 29 shows.

$$U(y) = 0{\cdot}5(1+\tanh 0{\cdot}5y).$$

The boundary conditions are as in the temporal case:

$$\phi(-\infty) = \phi(\infty) = 0.$$

† The theory is represented in dimensionless quantities.

As in the temporal case the complex eigenvalue $\alpha = \alpha_r + i\alpha_i$ and the complex eigenfunction $\phi = \phi_r + i\phi_i$ were computed numerically for some Strouhal numbers by Michalke (1965*b*), integrating the Rayleigh equation. Using the eigenvalues and

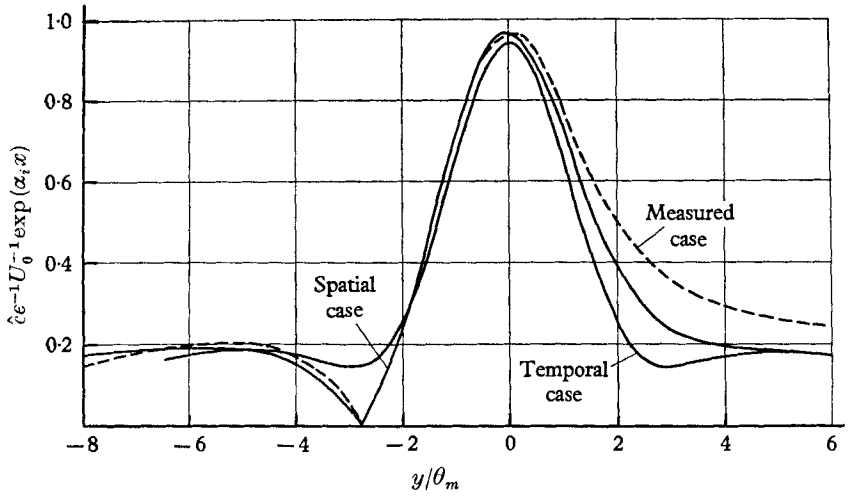

FIGURE 30. Theoretical and measured amplitude distribution for $S = 0{\cdot}008$.

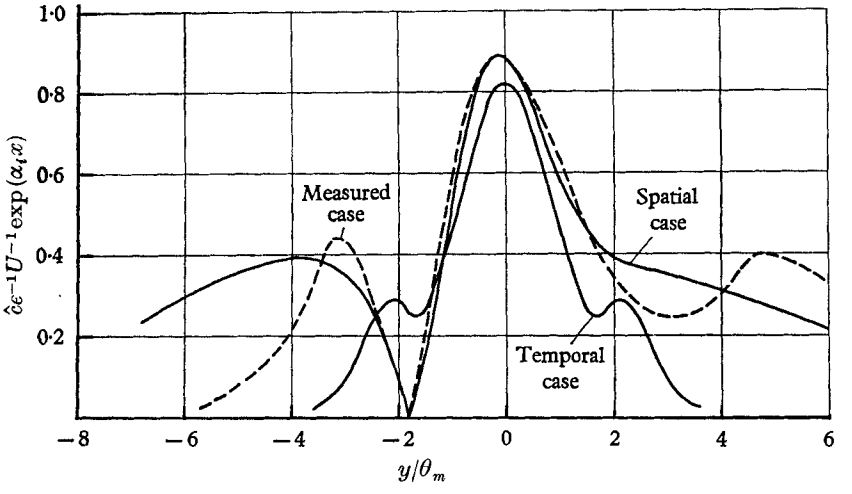

FIGURE 31. Theoretical and measured amplitude distribution for $S = 0{\cdot}017$.

functions for two different Strouhal numbers, the author calculated the amplitude and phase distribution for spatially as well as for temporally growing disturbances in order to compare them with the experiments. For the velocity fluctuations c/U_0 measured with the hot-wire approximately the following behaviour was obtained:

$$\frac{c}{U_0} \approx \frac{\partial \psi}{\partial y} = \epsilon e^{-\alpha_i x} \mathscr{R}[\phi' e^{i(\alpha_r x - 2\pi St)}].$$

Whence for the amplitude $\hat{c}/U_0$

$$\hat{c}U_0^{-1}\epsilon^{-1}\exp(\alpha_i x) = \sqrt{(\phi_r'^2 + \phi_i'^2)} \quad \text{amplitude distribution,}$$

and for the phase δ

$$\delta = \sin^{-1} \frac{\phi_i'}{\sqrt{(\phi_r'^2 + \phi_i'^2)}} \quad \text{phase distribution.}$$

The numerical results are given and compared with the experiments in the following section.

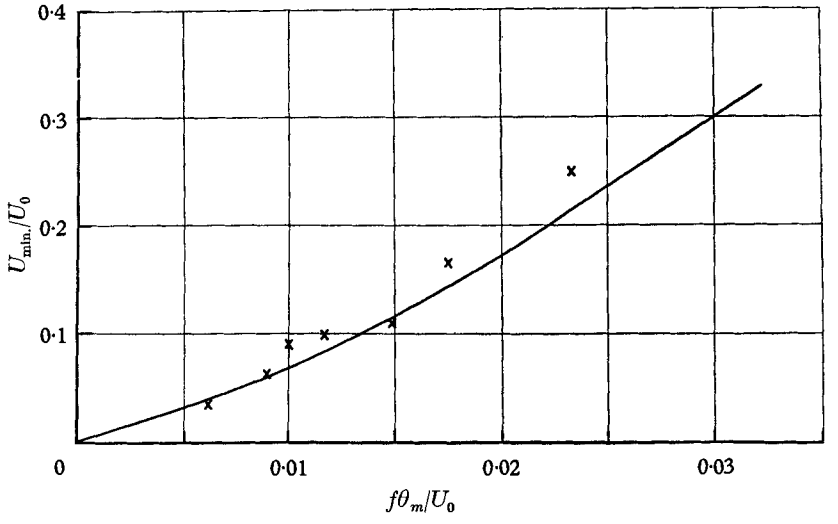

FIGURE 32. Theoretical and measured dependence of $U_{\min.}/U_0$ on the Strouhal number. $U_{\min.}$ is the mean velocity at the sharp minimum.

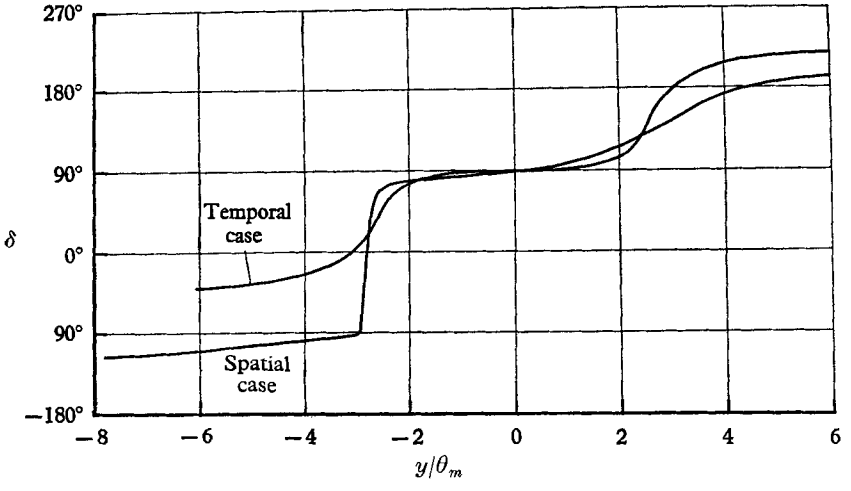

FIGURE 33. Theoretical phase distribution for $S = 0{\cdot}008$.

6.2. *Comparison of the calculated and the measured hot-wire analysis*

The amplitude and phase distribution were calculated for the Strouhal numbers $S = 0{\cdot}008$ and $S = 0{\cdot}017$ in the linear region. Figures 30 and 31 show the amplitude distribution for $S = 0{\cdot}008$ and for $S = 0{\cdot}017$ respectively for the temporal as well as for the spatial linearized theory. The measured amplitude distribution is

included, normalized in such a manner that the measured maximum $\hat{c}_2$ has the same value as in the spatial theory. We see that for the smaller Strouhal number the theoretical spatial curve agrees fairly well with the experimental curve. For the higher Strouhal number we find a difference caused by a third maximum in the

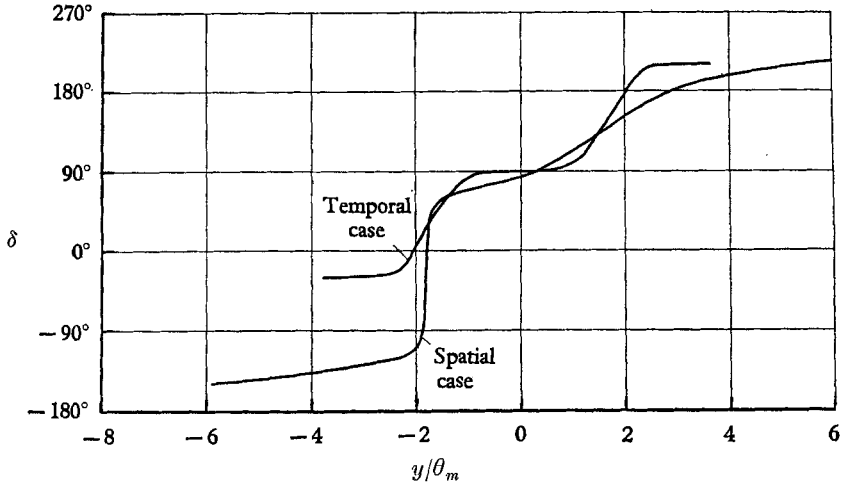

FIGURE 34. Theoretical phase distribution for $S = 0{\cdot}017$.

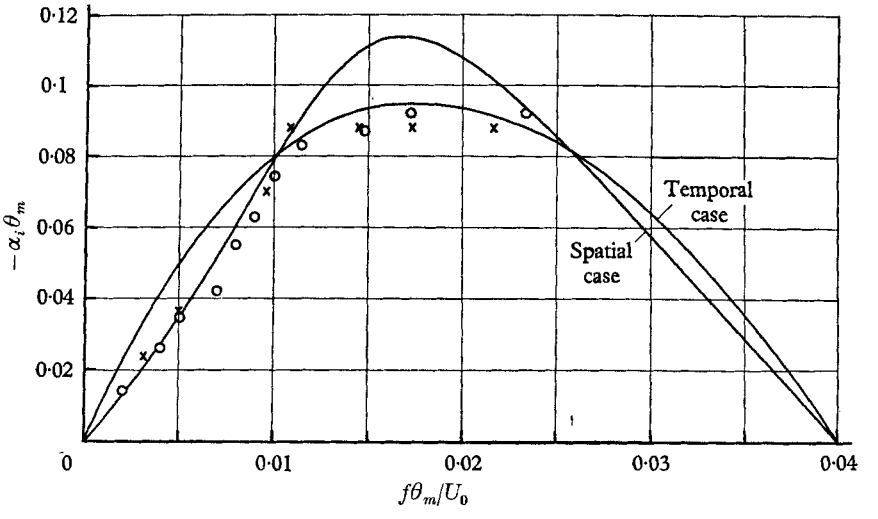

FIGURE 35. Growth rate $-\alpha_i\theta_m$ *vs.* Strouhal number.
○, Axisymmetric nozzle; ×, plane nozzle.

measured amplitude distribution. This third maximum is presumably caused by non-linear effects which for high Strouhal numbers are already present near the nozzle edge. The steeper slope beyond the smaller maximum is caused by the measuring method with hot-wires, since for high frequencies and small mean velocities there is a breakdown in the heat transfer from the hot-wire. The theoretical amplitude distributions in figures 30 and 31 show that with increasing Strouhal number the sharp minimum is shifted to the inner part of the layer, where the mean

velocity is higher. Furthermore, the ratio of the amplitude of the smaller maximum to the amplitude of the higher maximum increases with the Strouhal number. Both results were obtained by the experiments as well. This is shown in figures 32 and 22. Here too the agreement is good.

Figures 33 and 34 show the calculated phase distributions for the spatial and temporal case. We see that only for the spatial case does a sharp phase reversal occur at the position of the sharp minimum of the amplitude distribution. The measured phase distribution from figure 24 agrees qualitatively with the theoretical curves.

A further comparison was made concerning the growth rate $-\alpha_i \theta_m$ *vs.* Strouhal number. The curves calculated by Michalke (1965*b*) and the measured values are shown in figure 35. The measured values were obtained from the slopes of the curves of figures 16 and 21 in their linear region. There is a good agreement between spatial theory and experiment for $S < 0{\cdot}012$. For higher Strouhal numbers the agreement with the curve of temporal growing disturbances is even better. A similar result was obtained for the dependence of the wave-number on the Strouhal number (cf. figure 23).

The moderate discrepancy between the spatial theory and the experiments for high Strouhal numbers is presumably caused by non-linear effects, which cannot be described by the linearized theory and which have more importance for higher than for smaller Strouhal numbers. For Strouhal numbers higher than 0·025 the records could not be evaluated.

7. Causes of vortex break down

Since the viscosity has no effect on the transition in the investigated region of $61 \leqslant R_\theta \leqslant 334$, the beginning of vortex break down may not be characterized by a critical Reynolds number formed with the circulation of a single vortex $\Gamma_{\text{crit.}}$ as was suggested by Timme (1957). The vortex break down is presumably caused by the interaction of the vortices, i.e. by induction. This may be deduced from figure 1, where after slipping the vortices break down three-dimensionally.

This investigation was made as the author's Dr-Ing. thesis under the guidance of Professor Dr-Ing. R. Wille at the Institut für Turbulenzforschung of the Deutsche Versuchsanstalt für Luft- und Raumfahrt e.V. at Berlin. The author wishes to express his gratitude to Professor Dr-Ing. R. Wille, the Director of the Institute, and to Dr-Ing. A. Michalke, Dr-Ing. H. Schade and Dr-Ing. A. Timme for many stimulating discussions.

REFERENCES

Berger, E., Freymuth, P. & Froebel, E. 1963*a* Anwendung der Regeltechnik bei der Entwicklung eines CT-Hitzdrahtanemometers. *Deutche Versuchsanstalt f. Luftfahrt, Porz-Wahn, DVL-Rep.* no. 282/283.

Berger, E., Freymuth, P. & Froebel, E. 1963*b* Theorie und Konstruktion von CT-Hitzdrahtanemometern. *Konstruktion*, **15**, 495.

Brown, G. B. 1935 On vortex motion in gaseous jets and the origin of their sensitivity to sound. *Proc. Phys. Soc.* **47**, 703.

Domm, U. 1956 Über eine Hypothese, die den Mechanismus der Turbulenzentstehung betrifft. *Deutsche Versuchsanstalt f. Luftfahrt, Porz-Wahn, DVL-Rep.* no. 23.

FABIAN, H. 1960 Experimentelle Untersuchungen der Geschwindigkeitsschwankungen in der Mischungszone eines Freistrahles nahe der Düsenmündung. *Deutsche Versuchsanstalt f. Luftfahrt, Porz-Wahn, DVL-Rep.* no. 122.

GASTER, M. 1962 A note on the relation between temporally-increasing and spatially-increasing disturbances in hydrodynamic stability. *J. Fluid Mech.* **14**, 222.

GASTER, M. 1965 The role of spatially growing waves in the theory of hydrodynamic stability. *Progr. Aero. Sci.* **6**, 251.

GÖRTLER, H. 1940 Über eine dreidimensionale Instabilität laminarer Grenzschichten an konkaven Wänden. *Nachr. Wiss. Ges. Göttingen, Math. Phys. Kl., Neue Folge*, **2**, no. 1.

MICHALKE, A. 1962 Theoretische und experimentelle Untersuchung einer rotationssymmetrischen, laminaren Düsengrenzschicht. *Ing. Archiv*, **31**, 268.

MICHALKE, A. 1964 On the inviscid instability of the hyperbolic-tangent velocity profile. *J. Fluid Mech.* **19**, 543.

MICHALKE, A. 1965*a* Vortex formation in a free boundary layer according to stability theory. *J. Fluid Mech.* **22**, 371.

MICHALKE, A. 1965*b* Spatially growing disturbances in an inviscid shear layer. *J. Fluid Mech.* **23**, 521.

MICHALKE, A. & SCHADE, H. 1963 Zur Stabilität von freien Grenzschichten. *Ing. Archiv*, **33**, 1.

MICHALKE, A. & WILLE, R. 1966 Strömungsvorgänge im laminar-turbulenten Übergangsbereich von Freistrahlgrenzschichten. *Proc. 11th Intern. Congr. Appl. Mech., Munich*, 1964, (ed. H. Görtler). Berlin: Springer–Verlag.

REYNOLDS, O. 1883 An experimental investigation of the circumstances which determine whether the motion of water shall be direct or sinuous, and the law of resistance in parallel channels. *Phil. Trans. Roy. Soc.* **174**, 935.

SATO, H. 1956 Experimental investigation on the transition of a laminar separated layer. *J. Phys. Soc. Japan*, **11**, 702.

SATO, H. 1959 Further investigation on the transition of two-dimensional separated layer at subsonic speeds. *J. Phys. Soc. Japan*, **14**, 1797.

SATO, H. 1960 The stability and transition of a two-dimensional jet. *J. Fluid Mech.* **7**, 53.

SCHADE, H. 1962 Zur hydrodynamischen Stabilitätstheorie ebener und axialsymmetrischer Parallelströmungen. *Deutsche Versuchsanstalt f. Luftfahrt, Porz-Wahn, DVL-Rep.* no. 190.

SCHADE, H. & MICHALKE, A. 1962 Zur Entstehung von Wirbeln in einer freien Grenzschicht. *Z. Flugwiss.* **10**, 147.

SCHLICHTING, H. 1935 Amplitudenverteilung und Energiebilanz der kleinen Störungen bei der Plattenströmung. *Nachr. Wiss. Ges. Göttingen, Math. Phys. Kl., Fachgr.* **1**, 47.

SCHUBAUER, G. B. & SKRANSTAD, H. K. 1947 Laminar boundary layer oscillations and transition on a flat plate. *Nat. Bur. Stand. Res. Paper*, no. RP–1772.

TIMME, A. 1957 Über die Geschwindigkeitsverteilung in Wirbeln. *Ing. Archiv*, **15**, 205.

TIMME, A. 1959 Über Eigenschaften von Wirbel straßen. *Deutsche Versuchsanstalt f. Luftfahrt, Dorz–Wahn, DVL-Rep.* no. 77.

TOLLMIEN, W. 1929 Über die Entstehung der Turbulenz. 1. Mitt. *Nachr. Wiss. Ges. Göttingen, Math. Phys. Kl.* **21**.

WATSON, J. 1962 On spatially-growing finite disturbances in plane Poiseuille flow. *J. Fluid Mech.* **14**, 211.

WEHRMANN, O. 1957 Akustische Steuerung der turbulenten Anfachung im Freistrahl. *Jahrbuch Wiss. Ges. Luft- u. Raumfahrt*, WGL, 102.

WILLE, R. 1952 Über Strömungserscheinungen im Übergangsgebiet von geordneter zu ungeordneter Bewegung. *Jahrbuch Schiffbautechn. Ges.* **46**, 174.

WILLE, R. 1960 Modellvorstellungen zum Übergang Laminar-Turbulent. Arbeitsgemeinsch. *Forschung Nordrhein-Westfalen*, vol. **72**.

WILLE, R. 1963*a* Beiträge zur Phänomenologie der Freistrahlen. *Z. Flugwiss.* **11**, 222.

WILLE, R. 1963*b* Growth of velocity fluctuations leading to turbulence in free shear flow. *AFOSR Tech. Rep. Contract* AF 61 (052)-412, *Hermann-Föttinger-Inst.* TU Berlin.

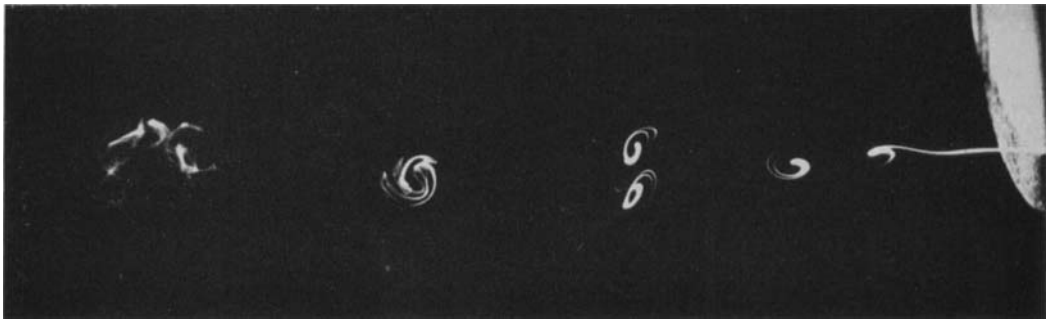

FIGURE 1. Instantaneous photograph of the rolling-up process of vortices, of slipping and coalescing of vortices, and of vortex disintegration. The smoke was introduced into the separated layer of an axisymmetric jet. $D = 7{\cdot}5$ cm, $U_0 = 3$ m/sec, $f = 95$ Hz.

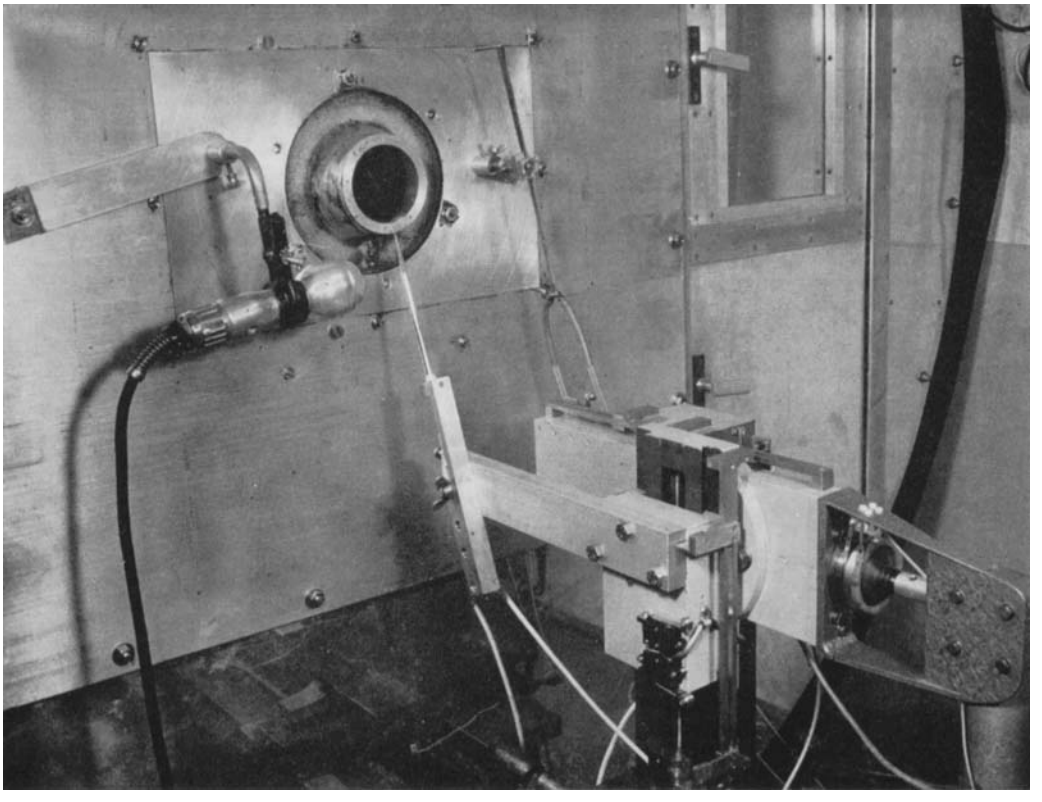

FIGURE 2. Part of the test stand with the hot-wire probe and its traversing mechanism.

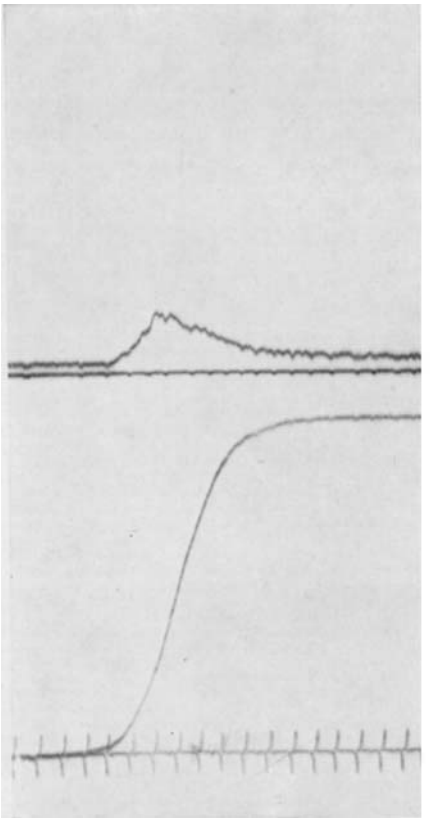

FIGURE 5. Velocity and amplitude distribution at $x = 0{\cdot}04$ cm for $D = 7{\cdot}5$ cm, $U_0 = 8$ m/sec, $f = 416$ Hz.

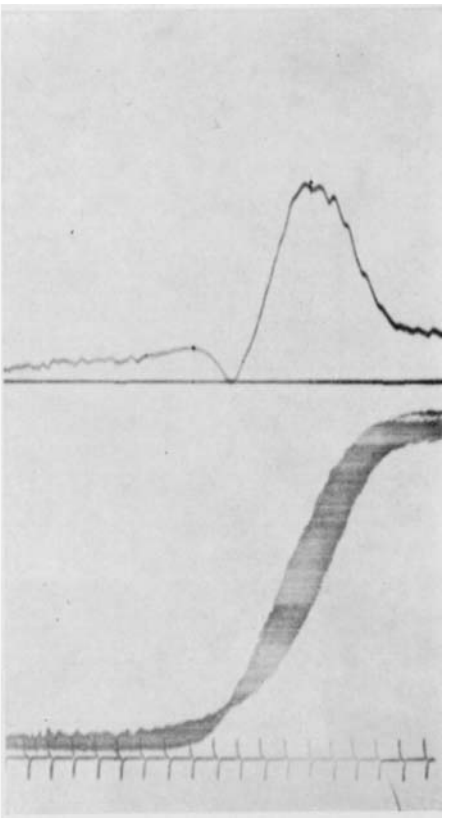

FIGURE 6. Velocity and amplitude distribution at $x = 1{\cdot}5$ cm for $D = 7{\cdot}5$ cm, $U_0 = 8$ m/sec, $f = 416$ Hz.

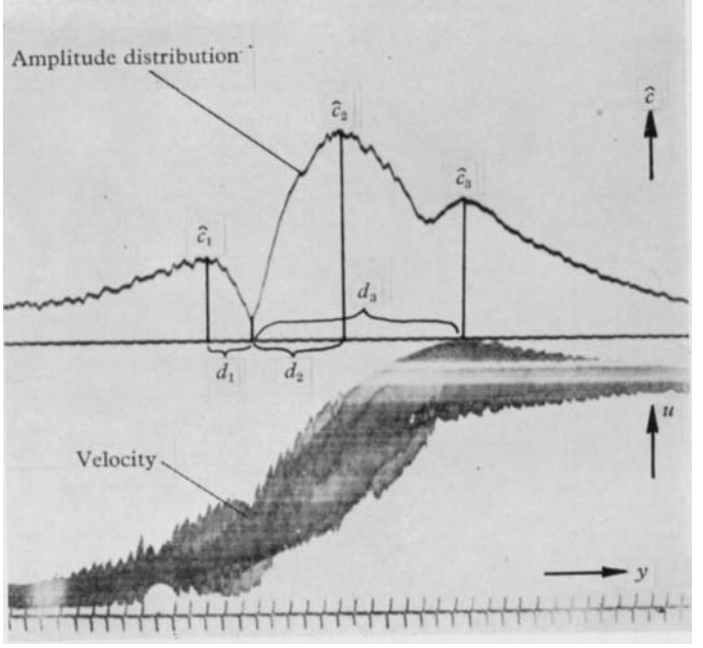

FIGURE 7. Velocity and amplitude distribution at $x = 2{\cdot}5$ cm for $D = 7{\cdot}5$ cm, $U_0 = 8$ m/sec, $f = 416$ Hz.

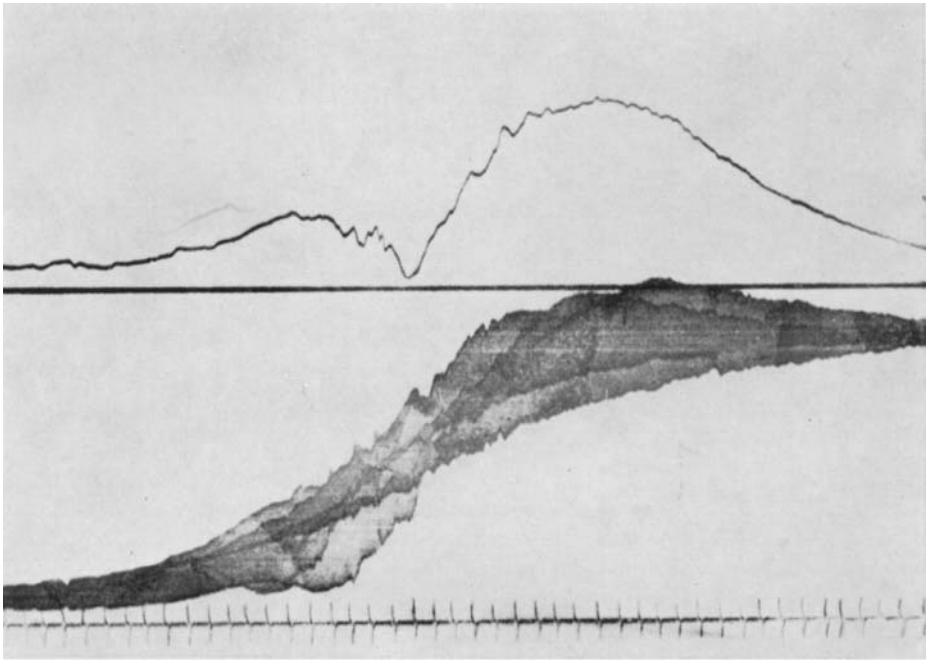

FIGURE 8. Velocity and amplitude distribution at $x = 3{\cdot}5$ cm for $D = 7{\cdot}5$ cm, $U_0 = 8$ m/sec, $f = 416$ Hz.

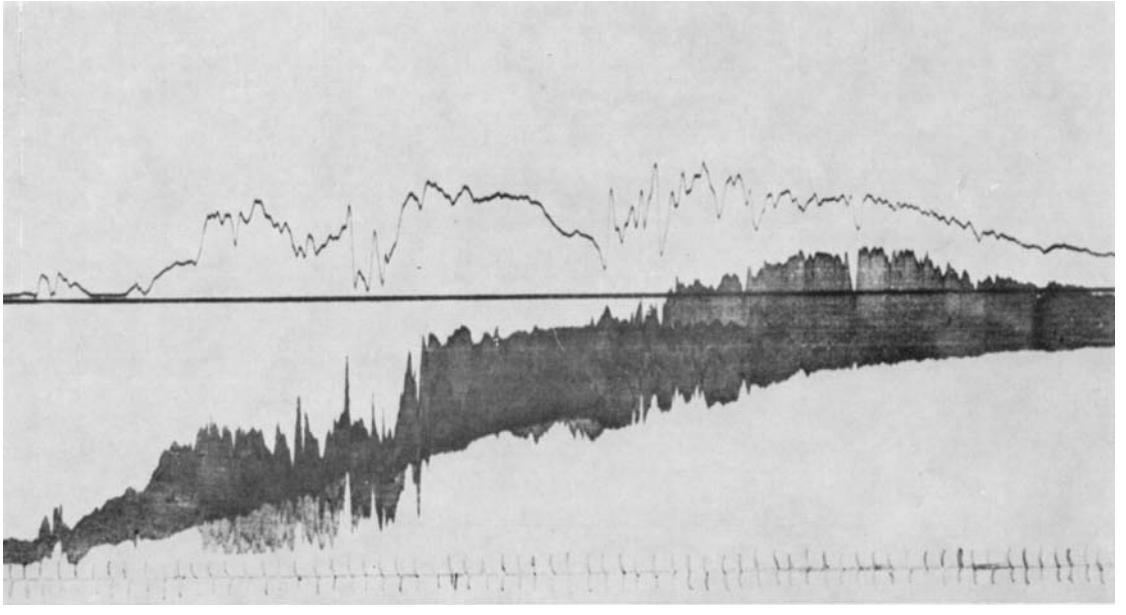

FIGURE 9. Velocity and amplitude distribution at $x = 4{\cdot}5$ cm for $D = 7{\cdot}5$ cm, $U_0 = 8$ m/sec, $f = 416$ Hz. The details of this figure are not reproducible.

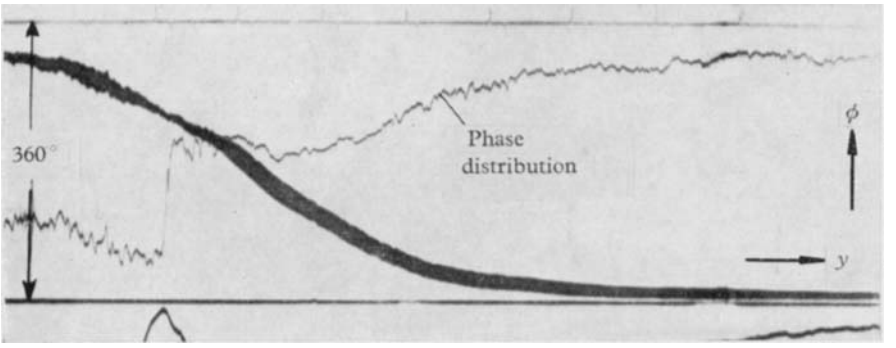

FIGURE 24. Phase distribution in the separated layer. $U_0 = 16$ m/sec, $S = 0{\cdot}018$. The inner part of the layer is on the right side of this figure.

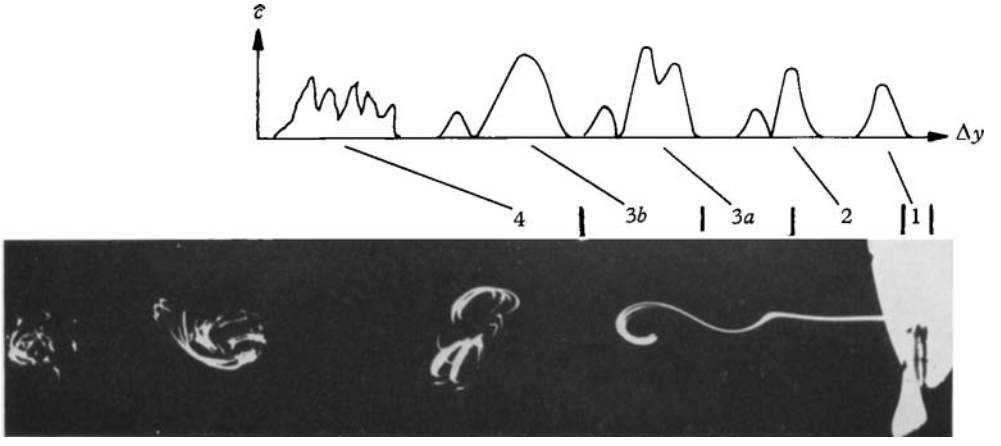

FIGURE 26. The four regions of transition: 1, transformation region; 2, region of linear transition; 3, region of non-linear transition; 4, turbulent region.

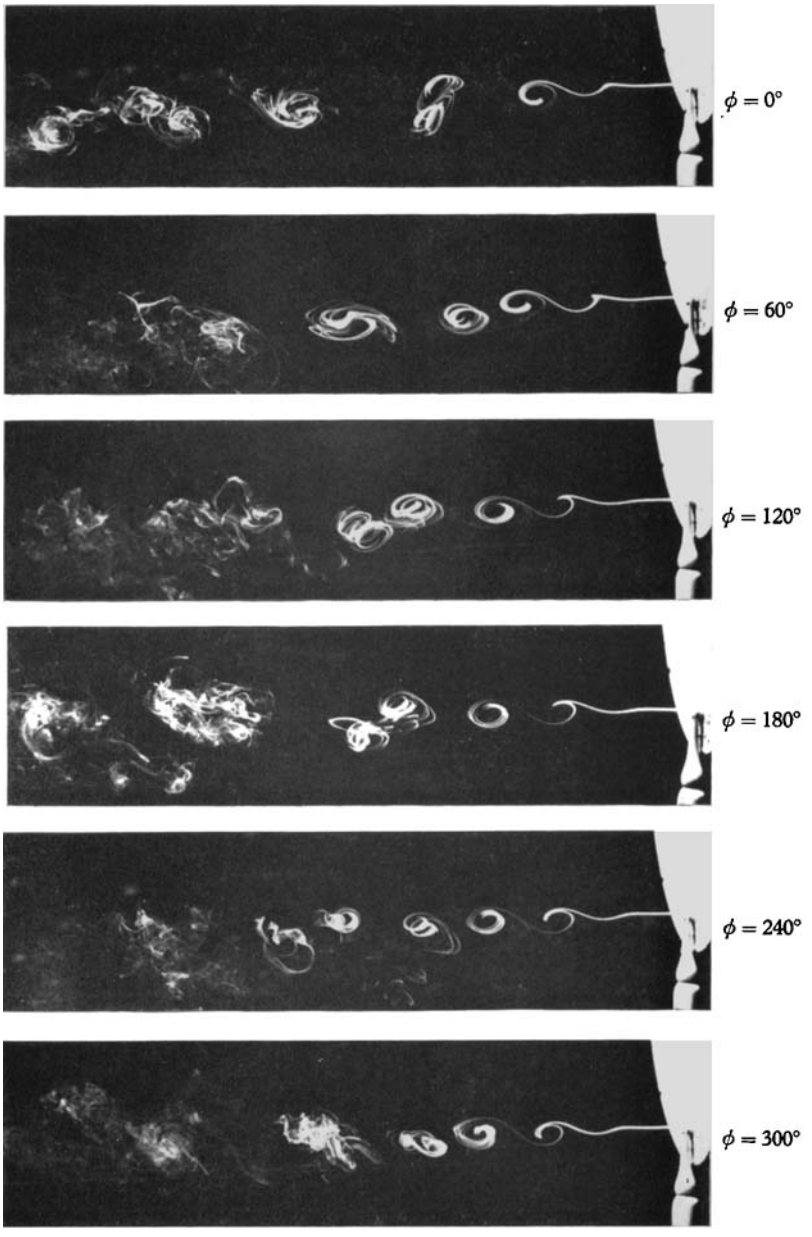

FIGURE 25. Stroboscopic smoke pictures, with a phase delay of $\Delta\phi = 60°$ from picture to picture. $D = 7{\cdot}5$ cm, $U_0 = 3$ m/sec, $f = 95$ Hz, $S = 0{\cdot}0118$.

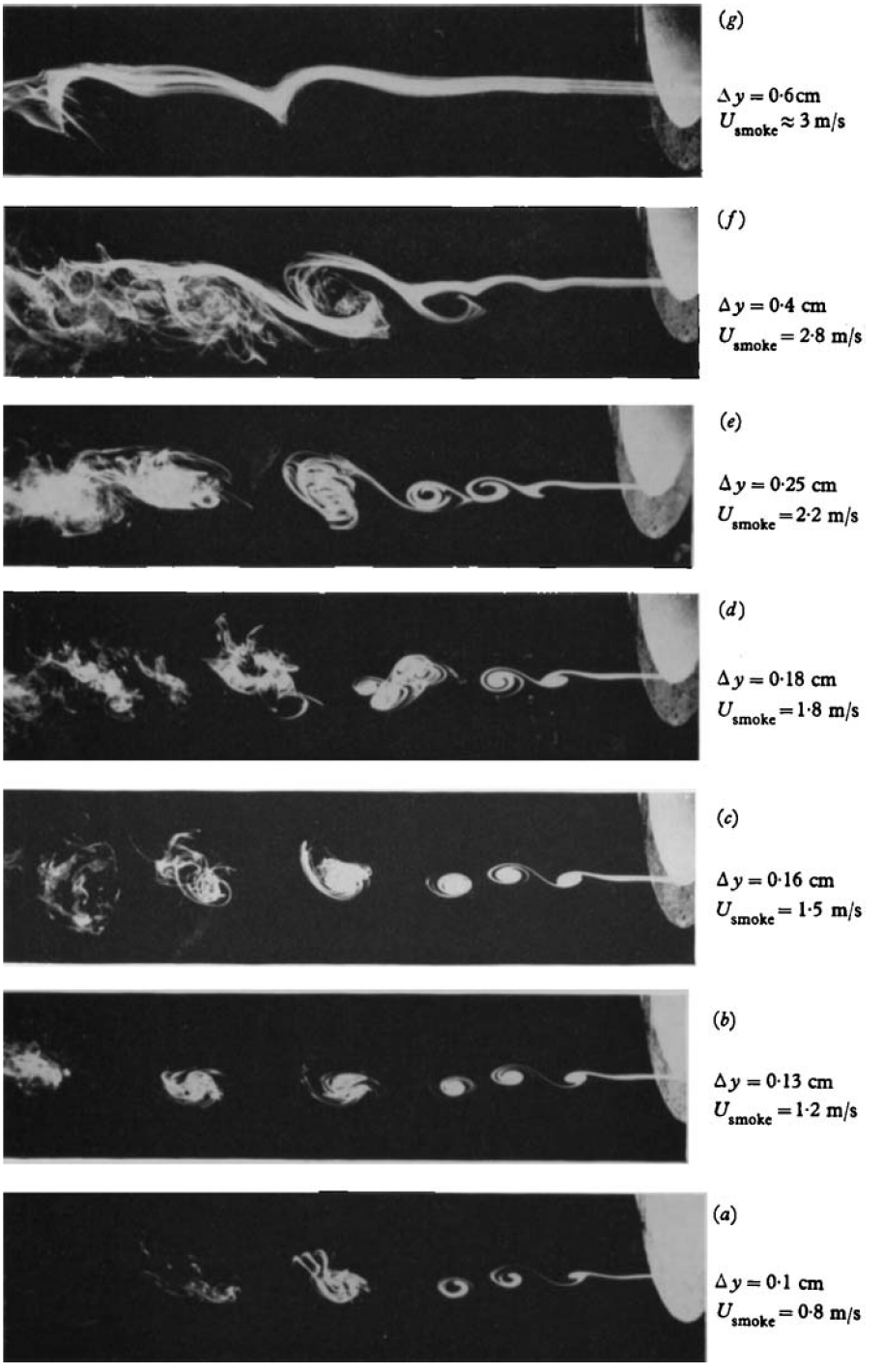

FIGURE 27. Smoke pictures; the smoke is introduced at various heights Δy. (Δy is the vertical distance of smoke from the nozzle edge.) $D = 7{\cdot}5$ cm, $U_0 = 3$ m/sec, $f = 95$ Hz, $S = 0{\cdot}0118$.

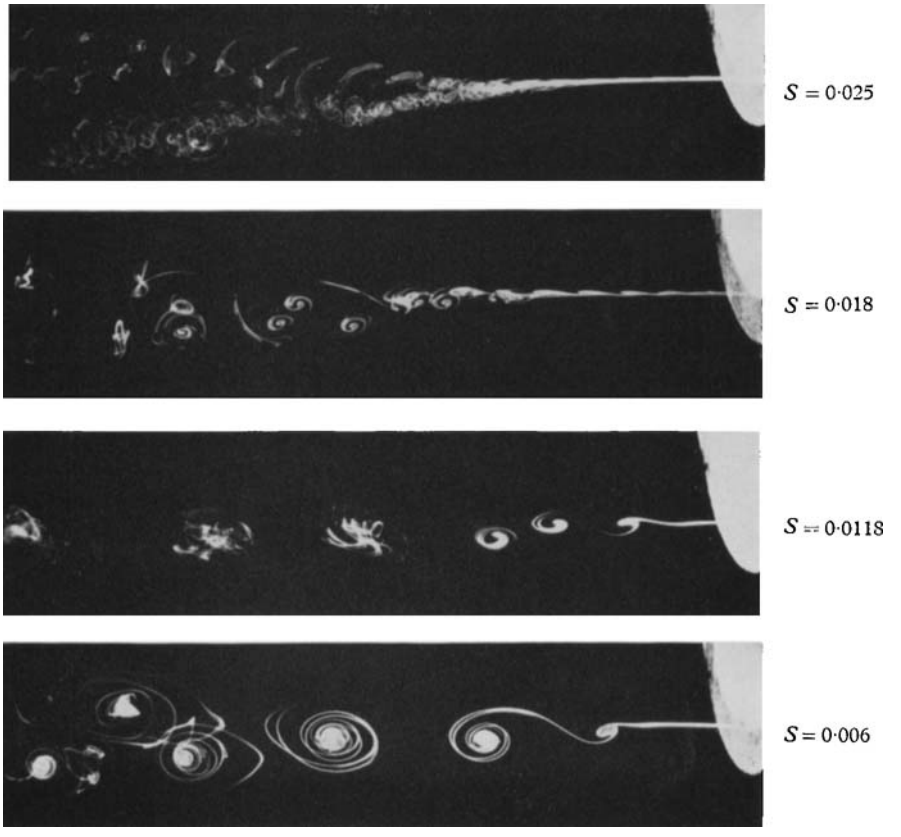

FIGURE 28. Dependence of the smoke picture on the Strouhal number.
$D = 7{\cdot}5$ cm, $U_0 = 3$ m/sec, $\Delta y = 0{\cdot}1$ cm.